Journal of Quantitative Spectroscopy & Radiative Transfer 242 (2020) 106798

Contents lists available at ScienceDirect

Journal of Quantitative Spectroscopy & Radiative Transfer

journal homepage: www.elsevier.com/locate/jqsrt

Revision of the 60-GHz atmospheric oxygen absorption band models for practical use

Dmitriy S. Makarov[a,*], Mikhail Yu. Tretyakov[a], Philip W. Rosenkranz[b]

[a] IAP RAS, 46 Ulyanov Str., Nizhny Novgorod 603950, Russia
[b] Massachusetts Institute of Technology, Cambridge, MA 02139, USA

ARTICLE INFO

Article history:
Received 13 August 2019
Revised 5 December 2019
Accepted 6 December 2019
Available online 16 December 2019

Keywords:
Microwave spectroscopy
Collisional coupling
Absorption model
Atmosphere
Molecular oxygen

ABSTRACT

Two models for millimeter-wave absorption by molecular oxygen in the air are updated. To derive the updated parameter set, earlier resonator spectrometer data are refined and recent data on the collisional parameters' temperature behavior are taken into account. The updated models provide significantly better agreement between laboratory measurements and calculated absorption band profiles than their earlier versions. The predictive ability of the models is confirmed by new experimental data. The covariance matrix of empirical parameter uncertainties, together with absorption-calculation uncertainty, are evaluated for both updated models. Contributions of the various sources to the total calculation uncertainty are discussed.

1. Introduction

The fine structure spectrum of molecular oxygen provides a significant part of the millimeter-wave radiation absorption in the Earth's atmosphere. Precise knowledge of the oxygen absorption coefficient in this spectral range is of great importance for atmospheric remote sensing, so models should be revised as spectroscopic improvements are made. The history of updating the shape of the single line near 118.75 GHz and the 60-GHz band can be tracked at [1–10]. The refinement of corresponding parameters of individual fine structure lines with increasing sensitivity of measurement technique is reported in [11–22].

The major feature of the fine structure spectrum of molecular oxygen at atmospheric conditions is a strong manifestation of the collisional coupling (line mixing) effect, which distorts the shape of the single 118-GHz line and significantly redistributes absorption within the 60-GHz band. As it was discussed in [10], the absorption profile depends on a collisional relaxation-operator matrix **W**. If there is no collisional coupling between lines, **W** is diagonal and the band profile turns into a sum of Van Vleck — Weisskopf profiles of the considered lines. When collisional coupling takes place, i.e. when off-diagonal **W** elements are not zero, the resulting absorption profile can be significantly different.

The elements of the matrix **W** can be calculated by various methods, e.g. directly by *ab initio* methods [23] or using analytical expressions for collisional cross-sections or basic rates together with measured broadening coefficients [24–26], or derived by numerical methods from the observed absorption profiles [16,18,27–29]. To evaluate the band profile, one may use direct numerical methods or in case of weak coupling (i.e. not too-high pressure), approximate it with an analytical expression by means of perturbation theory. Such approximation is used in the Millimeter-wave Propagation Model (MPM) [16,18,27,28,30], providing a simple analytical expression for fast calculation of the absorption coefficient in atmospheric air within a certain temperature and pressure range.

The latest improvement of the 60-GHz band profile suitable for MPM [29] used the perturbative approach to the band shape up to the second order of pressure [9]. First- and second-order mixing coefficients were derived by the Twomey-Tikhonov method for solution of ill-posed problems [31–33]. The same method was successfully used earlier, accounting only for the first-order mixing contribution [16,18,28]. Mixing coefficients derived in this way are valid only together with the particular set of basic parameters of the considered lines (intensity, central frequency, pressure broadening and shift coefficients) which are measured or calculated separately for each line; the most recent set of such self consistent line parameters was derived in [18].

Within the ECS (Energy Corrected Sudden) approach [24–26], matrix **W** obtained via calculation of the basic collisional rates together with direct numerical inversion is used to model the band profile. For the 60-GHz band, the matrix elements are calculated in [10] using analytical expressions for the basic rates, with

* Corresponding author.
E-mail address: dmak@ipfran.ru (D.S. Makarov).

https://doi.org/10.1016/j.jqsrt.2019.106798
0022-4073/

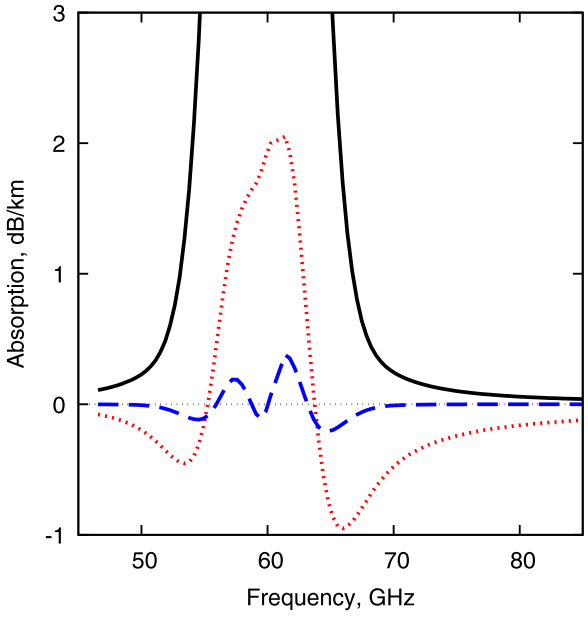

Fig. 1. First-order (red dotted curve) and second-order (blue dashed curve) corrections due to collisional coupling of the fine-structure lines of the 60-GHz band at 748 Torr and 300 K, calculated with MPM. Total absorption is shown with black curve, maximum is located near 61.39 GHz and corresponds to 13.31 dB/km. (For interpretation of the references to color in this figure legend, the reader is referred to the web version of this article.)

the model's adjustable parameter values determined by fitting the model profile to the profiles recorded at atmospheric pressures. Measured broadening coefficients are used for the matrix renormalization. This approach seems to be more physical, placing no restrictions on the matrix structure and applying numerical methods for the matrix inversion instead of perturbation theory, but it takes more computing resources.

The band-profile models are used for interpretation of radiometry measurements in the atmosphere. Paper [34] presents an experimental validation of the MPM version [18] (hereinafter referred to as "MPM-05") by means of multiple radiometric measurements at the low frequency wing of the band, supported by radiosonde data. A good agreement between observed and calculated brightness temperatures was demonstrated, especially for the 51.25 GHz channel where the second-order mixing correction becomes small and the first-order correction is sufficient (see Fig. 1). The validity of MPM-05 is also confirmed by its very good general agreement with the previous version of the model [16] which was based on measurement data obtained using a prepared dry air sample with a well-known oxygen concentration very close to the standard atmospheric value.

As it was expected, the aforementioned introduction of the second-order extension of MPM [29] (hereinafter referred to as "MPM-11") decreased systematic deviations of the model in the center of the band. However, later analysis of the model revealed minor (about 2–5%) systematic overestimation of the absorption in the far wings of the band, which can be observed, for example, in the ratio of spectra modeled by MPM-11 and MPM-05. This deviation pointed to the presence of systematic error in the measured band profiles used to derive the MPM-11 parameters accounting for the collisional coupling effect, and will be discussed in detail in this paper.

Section 2 of the current study is concerned with re-analysis of legacy experimental data and the general improvement of the 60-GHz absorption band modeling for practical use (Sections 2.1, 2.2 and 2.3, respectively), including verification of the modeling by new experimental data (Section 2.4). Section 3 is devoted to the evaluation of modeling uncertainties, including analysis of the band intensity value (Section 3.1) and correlations between parameters in MPM and ECS (Section 3.2). Section 4 summarizes the results of the study and gives the conclusion.

2. Absorption models revision

2.1. Refining the legacy measurements

The 60-GHz band profile recordings made by means of the resonator spectrometer [35] were used to derive the parameters for the previously reported MPM-11 [29] and ECS-based model [10]. The experimental setup and method were described in [29]. The gas chamber of the spectrometer was not designed as a vacuum cell so all measurements were carried out at ambient atmospheric pressure, slowly blowing the air first through a cold trap to remove water vapor, then through the chamber.

When the temperature drifts, the baseline spectrum changes. During the measurement cycle, temperatures of the mirrors and gas sample are permanently monitored and recorded. Using these temperature-versus-time recordings, one may eliminate the influence of minor temperature variations by calculation of the corresponding corrections for the resonator losses. Imperfection of such re-calculation introduces uncertainty of measured absorption, which may become significant when subtle effects are studied. The most difficult case is a long-time experimental cycle, when many factors (daily variation of laboratory temperature, variations of temperature gradients inside the chamber, etc.) may unpredictably affect the value of the instrumental losses. In this case empirical correction of the baseline may be necessary.

The collisional coupling effect between the lines forming a band does not change the band integrated intensity. Consequently, the average difference over the entire frequency range of the band, between measured absorption and that calculated by a verified model at the same conditions of temperature, pressure, and oxygen concentration, should be close to zero. Employing MPM-05 as a valid reference model, this criterion helped to define the oxygen concentration for the band profile recordings used in [29] and [10]. This method is equivalent to the common method of spectroscopic determination of absorbing molecules' concentration in gas mixtures using a known integrated intensity of an experimentally-observed line. First, absorption was calculated by means of MPM-05 [18] for the standard atmospheric oxygen concentration and measured values of temperature and pressure, and then the O_2 concentration was adjusted until the aforementioned intensity criterion had been satisfied. Observed-minus-calculated (obs.-calc.) residuals obtained in this way are shown in Fig. 2.

An important point is that at the edges of the band the residual also should tend to zero, because the band-shape distortion due to the second-order (and higher) coupling is expected to be weak at the edges and the difference between the first-order model and measurement should be negligibly small (Fig. 1). A closer look at the obs.-calc. residuals in Fig. 2 reveals that they deviate from zero for many recordings, presumably due to unaccounted baseline variations. These variations were not taken into account in [29], which introduced minor systematic errors in O_2 concentration. In the present study the primary experimental data were re-treated.

The unaccounted baseline can be approximated by a second-order polynomial based on the residual edges below 50 GHz and above 70 GHz. These polynomials are shown in Fig. 2 by red lines. Baselines determined in this way were subtracted from the band profile recordings before the further data treatment. Recall that troubles with the oxygen concentration in [29] were caused by using the liquid-nitrogen-cooled trap to dry the atmospheric air for the measurements. The temperature of liquid nitrogen at normal

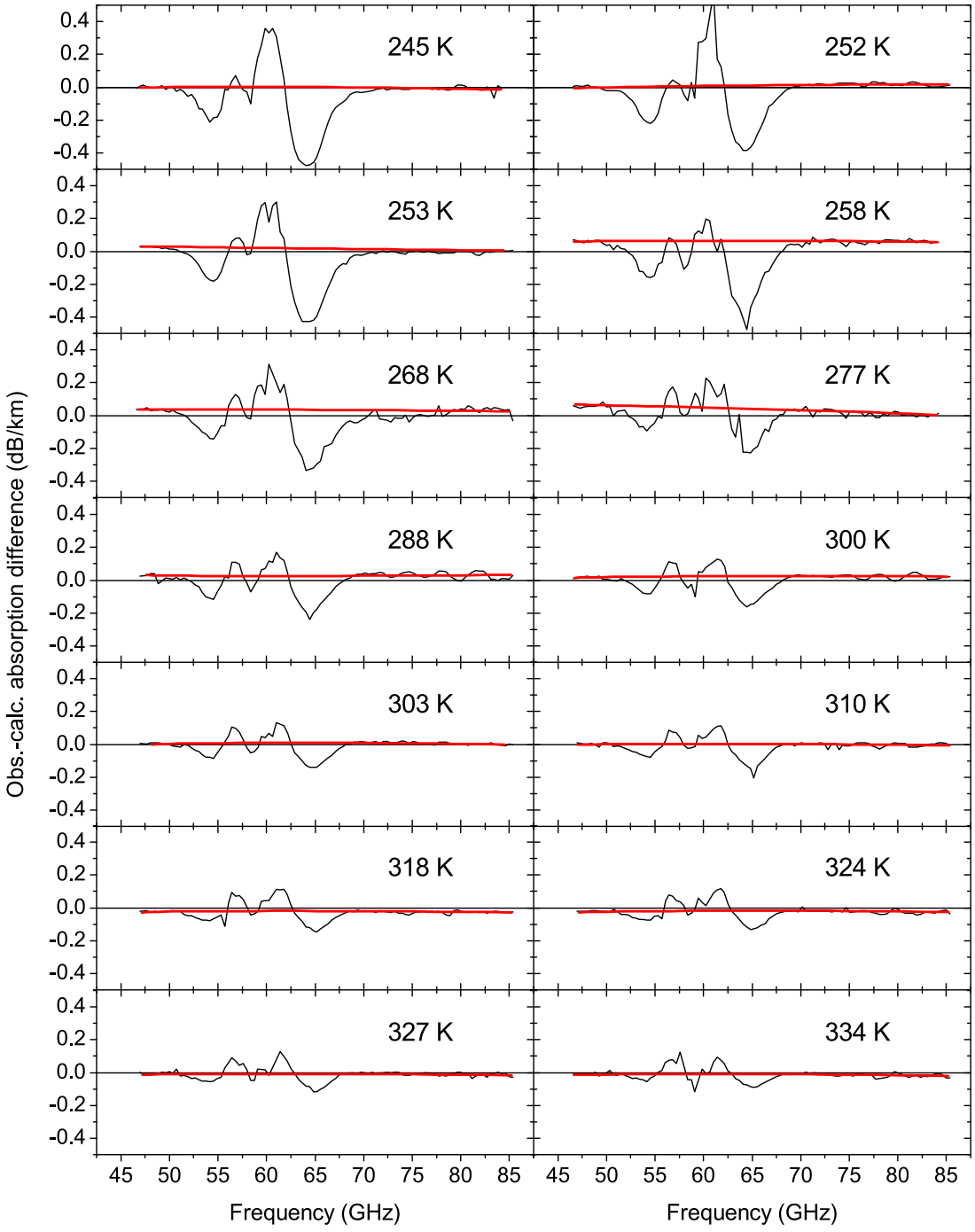

Fig. 2. Obs.-calc. absorption residuals at various temperatures, using the first-order mixing model MPM-05 [18] for calculation. The baseline contribution, unaccounted in [29], is shown by red lines. (For interpretation of the references to color in this figure legend, the reader is referred to the web version of this article.)

conditions is about 13 degrees lower than that for O_2 condensation. This may cause partial condensation of the oxygen inside the trap, reducing its concentration in the resonator chamber. Some excess of O_2 in the chamber is, in principle, possible due to the accumulated liquid O_2 evaporation but it is less probable, due to the regular refilling of the trap during the measurement cycle.

It is worth noting that the discussed corrections are small in comparison with the absorption near the band center (Fig. 3). Their magnitude is about ten times smaller than the difference between measured and MPM-05-calculated absorption, while that difference itself is 1-2% of the maximum absorption at the band center. Nevertheless, such a small correction leads to a noticeable change in the calculated absorption in the near and far wings, as it will be shown below.

The corrected oxygen concentrations and initial values from [29] are shown in Fig. 4. The refined concentration values are generally lower than the standard atmospheric value of 20.96%, which appears more reasonable in comparison to the initial values in view of the sample drying method used. Oxygen concentration values decreased on average by 0.3%, which corresponds to $\sim$1.5% change of the band intensity value. Note that this change is of the order of the uncertainty of the band intensity: a recent study

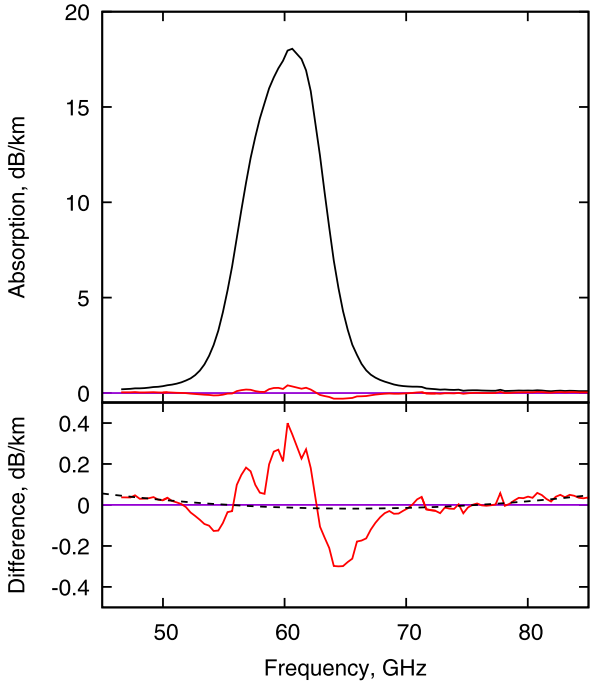

Fig. 3. Experimental recording of the band at 296 K and 755 Torr (upper panel) and difference between observed and calculated by MPM-05 [18] profiles. The dashed line shows the unaccounted baseline.

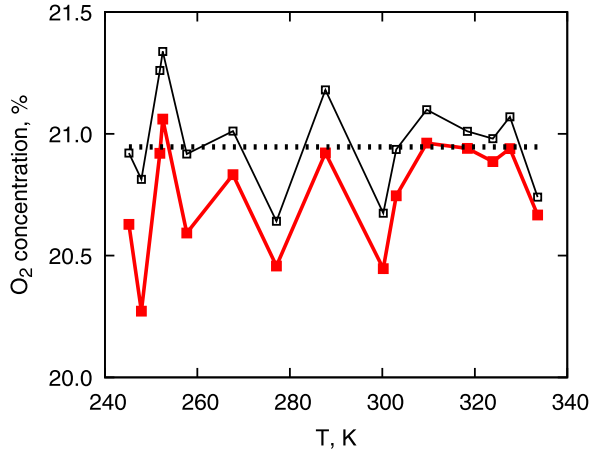

Fig. 4. Spectroscopically determined concentration of molecular oxygen in dry air at various temperatures before (black) and after (red) the baseline correction procedure. The standard atmospheric value is shown by the horizontal dotted line. (For interpretation of the references to color in this figure legend, the reader is referred to the web version of this article.)

[36] evaluated the uncertainty as ~1%, while in an earlier study [34] a value of 2% was accepted.

The corrected experimental spectra are attached to the current study [dataset][37]. They allow further refining of the collisional coupling parameters of the MPM and ECS-based models of the 60-GHz band, which is described in the two following subsections.

2.2. MPM update

The second-order MPM uses a line-by-line approach calculating the 60-GHz band profile as a sum of fine structure lines. Each line has a Van Vleck – Weisskopf profile [38] with the corrections due to the line mixing effect, proportional to pressure and pressure squared (see [9] and references therein for details). This requires three mixing parameters for each line. The first order parameter y introduces some line profile asymmetry, and the second order parameters g and $\delta\nu$ affect the line intensity and central frequency, respectively.

As mentioned above, the MPM first- and second-order mixing parameters are obtained by solution of the ill-posed inverse problem using the Twomey-Tikhonov method [16,18,28,29]. Although the method provides a set of 114 mixing parameters, the solution has effectively about four to five degrees of freedom (first mentioned in [16]). Accuracy of the experimental data is important, and this implies accuracy of (i) individual line basic parameters (intensities, central frequencies and broadening coefficients) and (ii) the band profile recordings at atmospheric pressure.

Some degree of freedom for the optimization procedure is provided by adjusting the Lagrange multiplier parameter β (see [16,18,28] for details). We use the Lagrange multiplier value normalized to the number of frequency points m in the spectrum recording, i.e. $\beta' = \beta/m$. This parameter is set manually and reducing its value results in smaller residuals between the observed and calculated absorption, which is not always physically justified and should be used cautiously.

In earlier studies, the credibility of the mixing-parameters set was determined through the smoothness of the dependence of the parameters on rotational quantum number N and analysis of the band profiles' obs.-calc. standard deviation [18]. However, the dependence of the mixing parameters on quantum number can be expected to be smooth within one spectral branch only if the branch does not overlap with the other branch which is collisionally coupled to the first one. This is not the case for the 60-GHz band, where non-smooth behavior of y parameters in the range of overlap of $N+$ and $N-$ branches was shown in [10] using the ECS approach. This allows trying smaller β' values for MPM optimization, providing better obs.-calc. residuals.

Multiple band profile recordings at various temperatures provide one more criterion for the credibility of the parameter set. As stated in earlier studies (e.g., [16,29] and references therein), the temperature dependence of mixing parameters can be approximated as

$$Z(T) = \left(Z^0 + Z^1\left(\frac{T_0}{T} - 1\right)\right) \cdot \left(\frac{T_0}{T}\right)^x \quad (1)$$

where T_0 is the reference temperature (usually 300 K) and Z is a substitution for any (y, g or $\delta\nu$) mixing parameter; upper indices 0 and 1 distinguish the parameter value at T_0 and its T-dependence. The optimization algorithm produces parameter values reduced to the exponential dependence $(T_0/T)^x$, leaving the remaining part of the dependence $Z^0 + Z^1(T_0/T - 1)$ to be fitted as a second step. So β' might be adjusted by looking at the quality of the T-dependence fitting to the values given by the optimization procedure. Smaller β' values provide better optimization residual for each particular band recording, but the corresponding mixing parameters might not have the expected T-dependence. A proper β' should give both reasonable optimization residuals and smooth T-dependence of the parameters.

In this study we used $x = 0.754$ from [22] for parameters γ (collisional broadening coefficient) and y, and $x = 1.508$ for second-order mixing parameters g and $\delta\nu$. This is justified by the following reasoning. The diagonal elements of **W** are the broadening coefficients, which are observed to depend on temperature as $(T_0/T)^{0.754}$ [22]. All elements of **W** are derived from the same intermolecular potential, so we assume that the off-diagonal elements contain this common factor of $(T_0/T)^{0.754}$. But the off-diagonal elements must also follow the detailed balance rule (Eq. (25) in [16]):

$$W_{lk} = W_{kl} \exp \frac{E_k - E_l}{k_B T} \quad (2)$$

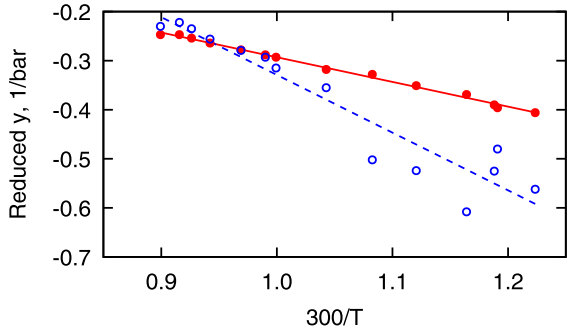

Fig. 5. Reduced by $(300/T)^x$ (see the text) first order mixing parameter values for the 13− line versus $(300/T)$, obtained by model optimization with $\beta' = 0.001$ (empty circles) and $\beta' = 0.1$ (filled circles). Corresponding fitted temperature dependences are shown by straight lines.

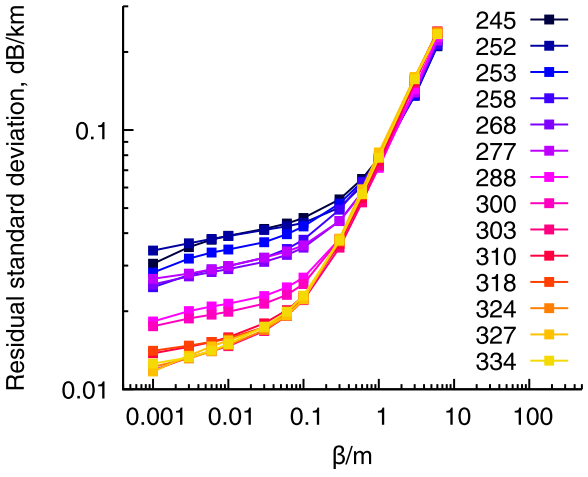

Fig. 6. Dependence of MPM optimization residuals' standard deviation on the normalized Lagrange multiplier β'. Values obtained at various temperatures are indicated by the corresponding color.

where E_k and E_l are energies of the lower level related to the lines k and l, respectively. The exponential in Eq. (2) can be approximated as $1 + (E_k - E_l)/k_BT$ when the energy levels are not widely separated. This implies that a term proportional to $(T_0/T)^{x+1}$ in addition to $(T_0/T)^x$ should be included in the temperature dependence of at least some of the off-diagonal matrix elements. First-order mixing parameters y are equal to weighted sums of off-diagonal elements of **W** (Eq. (15) in [9]). Thus, we use Eq. (1) with $x = 0.754$ for parameter y. The second-order mixing parameters g and $\delta\nu$ are weighted sums of pairwise products of **W** elements (see Eqs. (16) and (19) in [9]). Thus three terms appear, proportional to $(T_0/T)^{2x}$, $(T_0/T)^{2x+1}$ and $(T_0/T)^{2x+2}$. In practice, for atmospheric applications the third term is unnecessary, so our T-dependence model for the second order mixing parameters also follows Eq. (1), but the exponent value is doubled to $x = 1.508$.

By manual adjusting of β' we find that the optimal value is 0.1; this satisfies both criteria discussed above. The difference between $\beta' = 0.1$ and $\beta' = 0.001$ in terms of the second credibility criterion is shown in Fig. 5 — smaller β' provides non-regular T-dependence of y. In [18] the optimal β' value was suggested to be near the "knee" of the dependence, where slow growth of the residual changes to fast growth (Fig. 10 from [18]). Looking at the same dependence for the present data (Fig. 6), one may note that $\beta' = 0.1$ is in good agreement with this criterion as well.

Fig. 7 demonstrates the improvement in the model optimization to individual band recordings. Mean values and standard deviations of the residuals between the experimental data and the optimized model are shown for both refined (as described in Section 2.1) and initial data. Optimization of MPM to the refined 60-GHz band profiles provides residuals with mean value close to zero (generally smaller than 0.01 dB/km corresponding to random experimental noise), and the standard deviation of all residuals decreases. The improvement reaches a factor of 1.5 at lower temperatures, where manifestation of line mixing is more pronounced than at temperatures above 300 K.

Residuals between the experimental data and optimized MPM are shown in Fig. 8. Improvement of the absorption data leads to more uniform and "concentrated" residuals, having a similar shape of the minor remaining systematic deviations, with decreasing magnitude at higher temperature. Mixing parameters derived from the refined data (Fig. 9) noticeably differ from the ones derived from the initial data. The first-order parameters y^0 (Z^0 parameter of Eq. (1)) corresponding to the refined data are in better agreement with values found earlier in [18] which are also shown in Fig. 9 for comparison, than values from [29] are. The updated MPM parameter-values and their statistical uncertainties derived from the temperature-dependence fit are given in Table 1. Air broadening values used for the optimization (updated according to [22]) and line intensities (retained from the previous models [18,29]) are also given in Table 1 because mixing, broadening and intensity parameters are correlated and should be considered as a self-consistent set of data, as noted in [18]. The correlation of parameters and the related uncertainty of the modelling will be discussed in Section 3 of this study.

2.3. ECS update

Within the ECS approach, elements of the relaxation matrix are based on the so-called basic rates $Q_L(T)$, adiabaticity factors and *a priori* known broadening coefficients [24,25]. The basic rates are calculated through an analytical EP law expression containing three empirically adjusted parameters to describe the dependence of the rates on quantum number. Renormalization of the matrix elements [39] allows reduction of the number of parameters to two. These parameters in Eqs. (7),(8) from [10] were denoted as α and β (but here we follow notation from [26] and use λ instead of α). A last parameter d_c, included in the adiabaticity factor (Eq. (8) of [10]) is tied to the effective duration of the collision. Parameter β is interpreted as a fraction of rotational energy transmitted in a collision, and λ introduces a general decrease of the basic rate versus quantum number (the interested reader is referred to [24,40,41]). The ECS-based band model can be directly fitted to the refined experimental data by means of the Levenberg-Marquardt algorithm [42], in the same way as model profiles of single lines. Degrees of freedom in the fitting procedure correspond in this case to the number of variable parameters.

Residuals of the recording-by-recording fit of the ECS model are shown in Fig. 10. This result is similar to the one obtained with MPM: residuals are smaller in magnitude and are close to zero on the wings, which is confirmed by the calculated mean and standard deviation values of the corresponding residuals, in Fig. 11.

Parameters of the ECS model derived from fitting and averaged over all temperature values are λ_{new}=0.39(2), β_{new}=0.567(5), $d_{c(new)}$=0.61(1) Å (1-σ statistical uncertainty is given in parentheses in terms of the last significant digit). Corresponding values from [10] were $\lambda_{old} \approx 0.32(2)$ (in [10] this parameter has unexpected weak temperature dependence; new values do not reveal such dependence), $\beta_{old} = 0.57(1)$, $d_{c(old)}$=0.54(2) Å. All related data are shown in Fig. 12. Note that old and new λ and d_c parameters coincide with each other within a 3-σ interval. Old and new β parameters coincide within 1-σ.

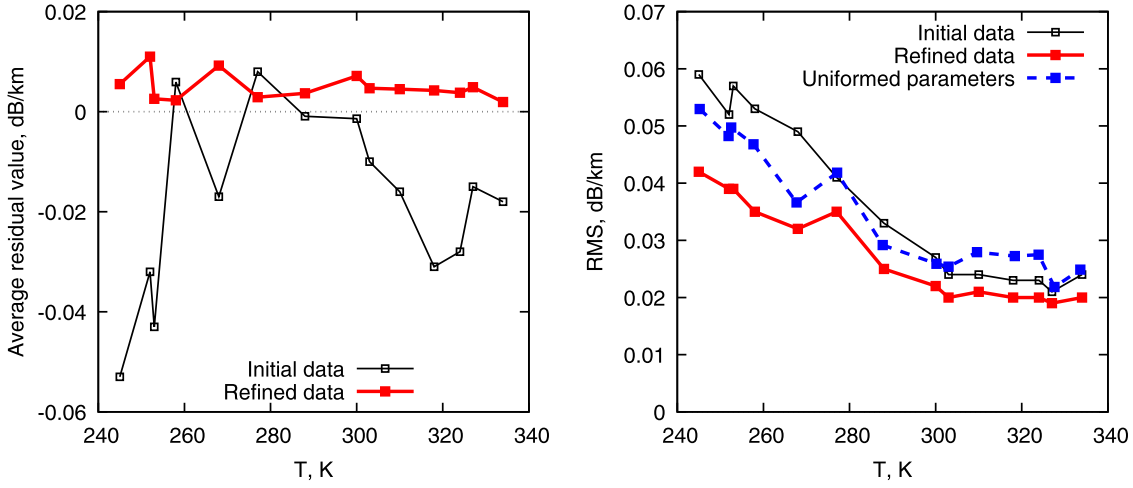

Fig. 7. Results of the MPM optimization to initial [29] and refined experimental recordings: mean values of the optimization residual at corresponding temperatures (left) and residuals' standard deviations (right). The uniformed parameters are calculated by fitting to Eq. (1).

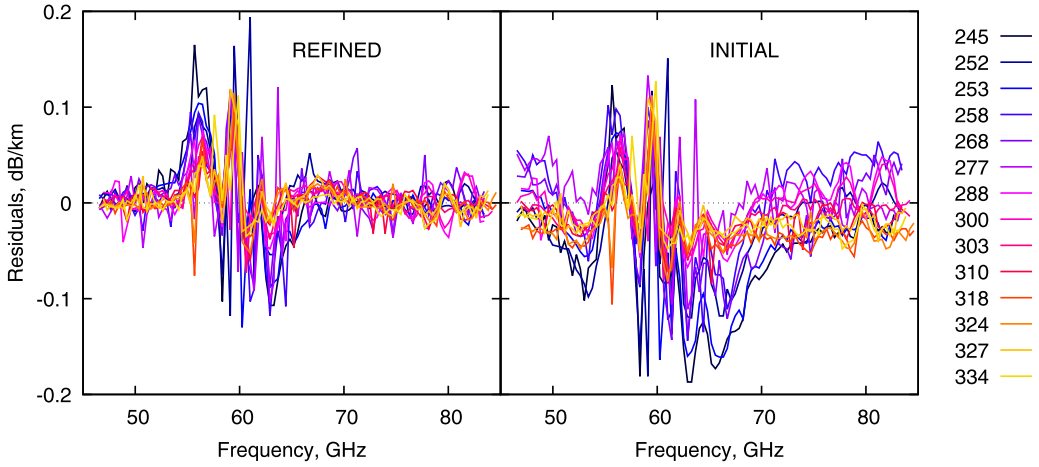

Fig. 8. Recording-by-recording MPM optimization residuals for refined (left) and initial [29] (right) experimental recordings. Curve colors correspond to temperatures shown on the right.

2.4. Model comparison and verification

Recording-by-recording optimization of both models to the refined experimental data gives parameter values suitable for the particular experimental temperature. From these values, uniformed parameter values suitable for all temperatures are derived. For the ECS model, averaged values corresponding to the solid lines in Fig. 12 are used. For MPM, two terms for each line-mixing parameter were used, as given by Eq. (1).

Using these uniformed values, the difference between measured and calculated absorption was obtained. Corresponding standard deviations are shown in Figs. 7 and 11 by the dotted lines, revealing no significant difference from the result of the model fit to individual recordings.

To verify models, two test recordings of the 60-GHz band profile were used. Modifications of the spectrometer since the year of 2011 included introduction of a vacuum chamber for the gases being studied and significant increase of the spectral scanning speed. The general method of measurements remained the same as described in [29]. More details about the spectrometer can be found in [43].

The spectra were recorded at four different distances between the radiation source and the resonator. This reduces unavoidable remaining standing waves in the spectrometer, which affect the instrumental baseline, and thus increases sensitivity to absorption [43]. Pure argon was used for the baseline recordings.

An artificial air mixture was prepared inside the spectrometer chamber using pure molecular nitrogen, molecular oxygen and argon (the local supplier specified the purity of all samples as not worse than 99.999%). The band recordings were made at 750 Torr and 1000 Torr at temperatures 295.8 K and 296.0 K respectively. Note that absorption modeling at 1000 Torr constitutes extrapolation because the parameters of the models were determined from the results of previous measurements performed at atmospheric pressures (within 735–760 Torr), but at 1000 Torr the line-mixing effect should be more pronounced.

The MPM and ECS models with updated parameters were used to calculate absorption coefficients at the measured pressures and temperatures, without optimizing the models to this new data. The oxygen concentration was determined spectroscopically from the data using MPM-05 [18] as described in Section 2.1, to ensure adequate comparison of spectral details related to line mixing and to exclude common problems of partial pressure determination in gas mixtures related to preferential adsorption, uncertainties of pressure gauges, gas purity, etc. The mixture was prepared with partial pressure of the molecular oxygen corresponding to the standard concentration value of 20.96%. The retrieved concentration values are 20.61(11)% at 750 Torr and 20.66(18)% at 1000 Torr.

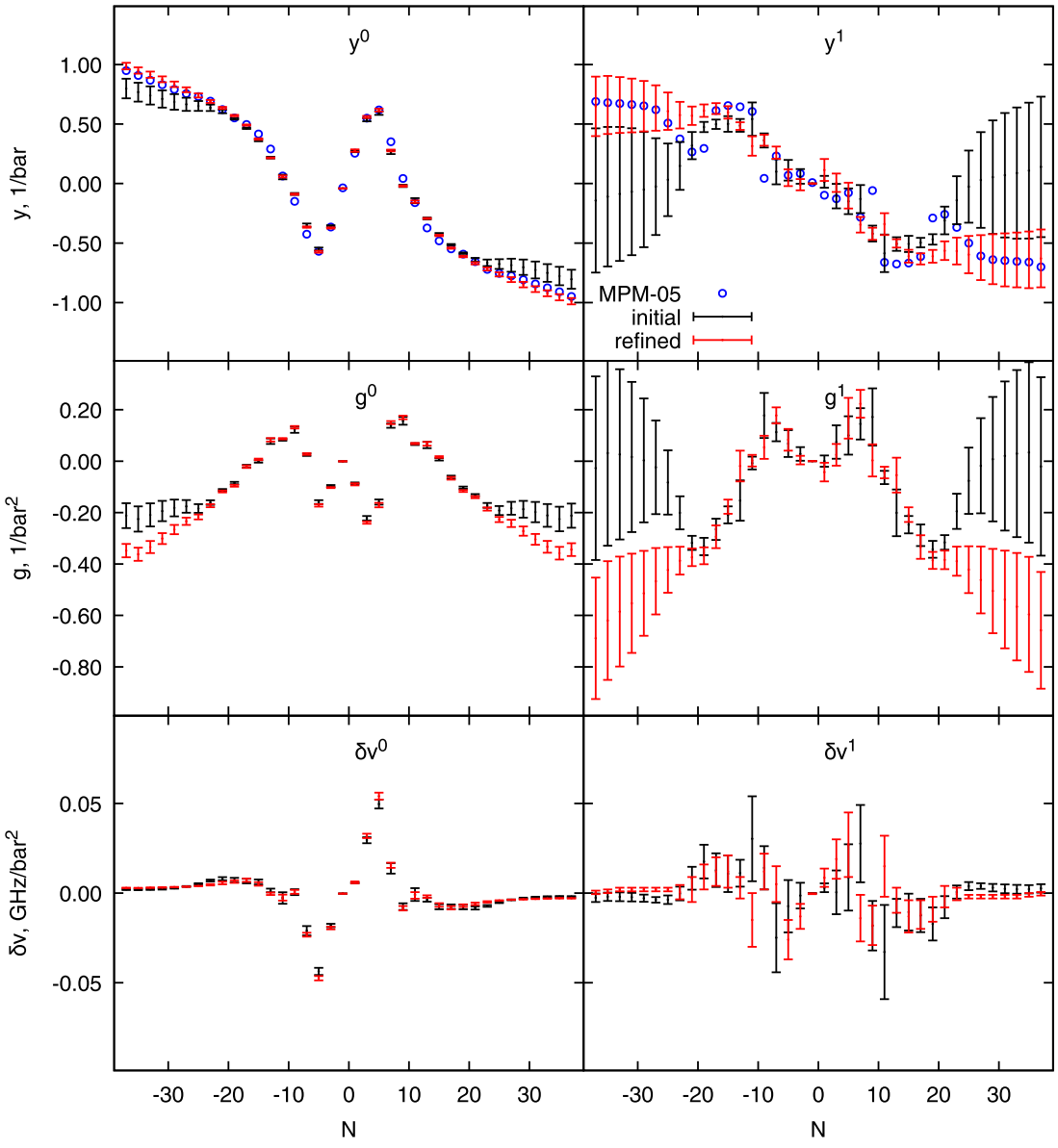

Fig. 9. First-order (y) and second-order (g and $\delta\nu$) mixing parameters derived from refined (red) and initial [29] (black) data versus transition notation N. Left side shows parameters Z^0, right side — parameters Z^1 in terms of Eq. (1). For the first-order parameters, values from the first-order MPM [18] are shown by blue circles. (For interpretation of the references to color in this figure legend, the reader is referred to the web version of this article.)

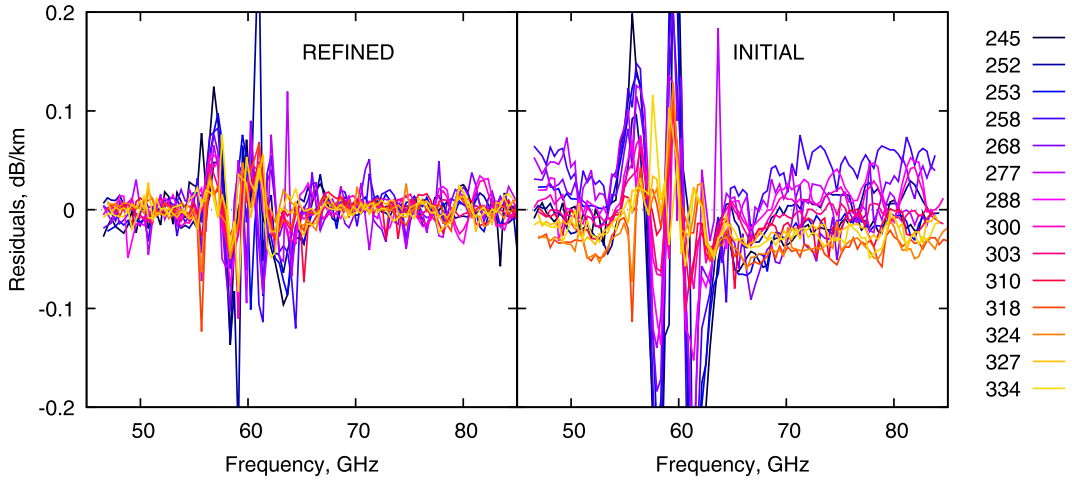

Fig. 10. Recording-by-recording residuals of the ECS model fit to the refined (left) and initial [10,29] (right) experimental recordings. Curve colors correspond to temperatures shown on the right.

Table 1
Mixing parameters for the fine structure O_2 transitions derived from MPM-optimization to the refined 60-GHz band recordings in dry air, together with corresponding intensities and broadening coefficients used for the optimization.

N	Intensity, 10^6 kHz/kPa	γ_{air}, GHz/bar	y^0, 1/bar	y^1, 1/bar	g^0, 1/bar^2	g^1, 1/bar^2	$\delta\nu^0$, GHz/bar^2	$\delta\nu^1$, GHz/bar^2
1-	940.3	1.685	−0.041(2)	0	−0.000695(7)	0.	−0.00028(2)	−0.00039(18)
1+	543.4	1.703	0.277(10)	0.124(73)	−0.090(4)	-0.045(28)	0.00597(54)	0.009(4)
3-	1503.0	1.513	−0.372(5)	−0.002(38)	−0.103(2)	0.007(13)	−0.0195(8)	−0.012(6)
3+	1442.1	1.495	0.559(9)	0.008(64)	−0.239(5)	0.033(35)	0.032(1)	0.016(9)
5-	2103.4	1.433	−0.573(7)	0.045(55)	−0.172(4)	0.081(33)	−0.0475(12)	−0.027(9)
5+	2090.7	1.408	0.618(12)	−0.093(84)	−0.171(8)	0.162(62)	0.0541(19)	0.029(14)
7-	2379.9	1.353	−0.366(6)	0.264(40)	0.028(3)	0.179(24)	−0.0232(11)	0.006(8)
7+	2438.0	1.353	0.278(7)	−0.351(52)	0.150(6)	0.225(42)	0.0154(14)	−0.015(10)
9-	2363.7	1.303	−0.089(5)	0.359(37)	0.132(5)	0.054(35)	0.0007(11)	0.010(8)
9+	2479.5	1.319	−0.021(6)	−0.416(40)	0.170(7)	0.003(48)	−0.0084(12)	−0.014(9)
11-	2120.1	1.262	0.060(9)	0.326(65)	0.087(2)	0.0004(180)	−0.0025(17)	−0.013(12)
11+	2275.9	1.265	−0.152(10)	−0.353(73)	0.069(2)	−0.047(18)	−0.0014(18)	0.013(13)
13-	1746.6	1.238	0.216(3)	0.484(25)	0.083(7)	−0.034(52)	−0.0004(7)	0.004(5)
13+	1915.4	1.217	−0.293(4)	−0.503(27)	0.067(8)	−0.071(58)	−0.0020(7)	−0.005(5)
15-	1331.8	1.207	0.373(7)	0.579(51)	0.007(3)	−0.180(23)	0.005(1)	0.010(8)
15+	1490.2	1.207	−0.436(7)	−0.590(53)	0.016(3)	−0.210(22)	−0.0066(11)	−0.010(8)
17-	945.3	1.137	0.491(6)	0.616(42)	−0.021(5)	−0.285(38)	0.0072(9)	0.010(7)
17+	1078.0	1.137	−0.542(6)	−0.619(43)	−0.066(5)	−0.323(40)	−0.008(1)	−0.011(7)
19-	627.1	1.101	0.571(6)	0.611(41)	−0.095(4)	−0.363(27)	0.0064(7)	0.008(5)
19+	728.7	1.101	−0.613(6)	−0.609(42)	−0.115(4)	−0.380(27)	−0.0070(7)	−0.009(5)
21-	389.7	1.037	0.636(8)	0.574(60)	−0.118(4)	−0.378(27)	0.0056(7)	0.003(5)
21+	461.3	1.038	−0.670(8)	−0.568(61)	−0.140(4)	−0.387(28)	−0.0060(7)	−0.003(5)
23-	227.3	0.996	0.690(12)	0.574(86)	−0.173(6)	−0.392(43)	0.0047(4)	0.0009(30)
23+	274.0	0.996	−0.718(12)	−0.566(87)	−0.186(6)	−0.394(44)	−0.0049(4)	−0.0009(30)
25-	124.6	0.955	0.740(17)	0.60(12)	−0.217(9)	−0.424(69)	0.0040(1)	0.0017(9)
25+	153.0	0.955	−0.763(17)	−0.59(12)	−0.227(10)	−0.422(70)	−0.0041(1)	−0.0016(9)
27-	64.29	0.906	0.788(20)	0.63(15)	−0.234(14)	−0.465(100)	0.0036(1)	0.0024(8)
27+	80.40	0.906	−0.807(20)	−0.62(15)	−0.242(14)	−0.46(10)	−0.0037(1)	−0.0023(8)
29-	31.24	0.858	0.834(23)	0.64(16)	−0.266(18)	−0.51(13)	0.0033(1)	0.0024(9)
29+	39.80	0.858	−0.849(22)	−0.63(16)	−0.272(17)	−0.50(13)	−0.0034(1)	−0.0024(9)
31-	14.32	0.811	0.876(24)	0.65(17)	−0.301(21)	−0.55(15)	0.0032(1)	0.0024(9)
31+	18.56	0.811	−0.887(25)	−0.64(17)	−0.304(20)	−0.54(15)	−0.0032(1)	−0.0020(9)
33-	6.193	0.764	0.915(25)	0.65(18)	−0.334(23)	−0.58(17)	0.0030(1)	0.0017(9)
33+	8.172	0.764	−0.922(25)	−0.64(18)	−0.333(23)	−0.56(16)	−0.0030(1)	−0.0016(9)
35-	2.529	0.717	0.950(26)	0.65(19)	−0.361(25)	−0.62(18)	0.0028(1)	0.0013(8)
35+	3.397	0.717	−0.955(25)	−0.64(18)	−0.358(24)	−0.59(17)	−0.0029(1)	−0.0012(8)
37-	0.975	0.669	0.987(27)	0.64(19)	−0.348(25)	−0.68(18)	0.0029(1)	0.0005(8)
37+	1.334	0.669	−0.988(26)	−0.62(19)	−0.344(24)	−0.65(18)	−0.0029(1)	−0.0004(8)

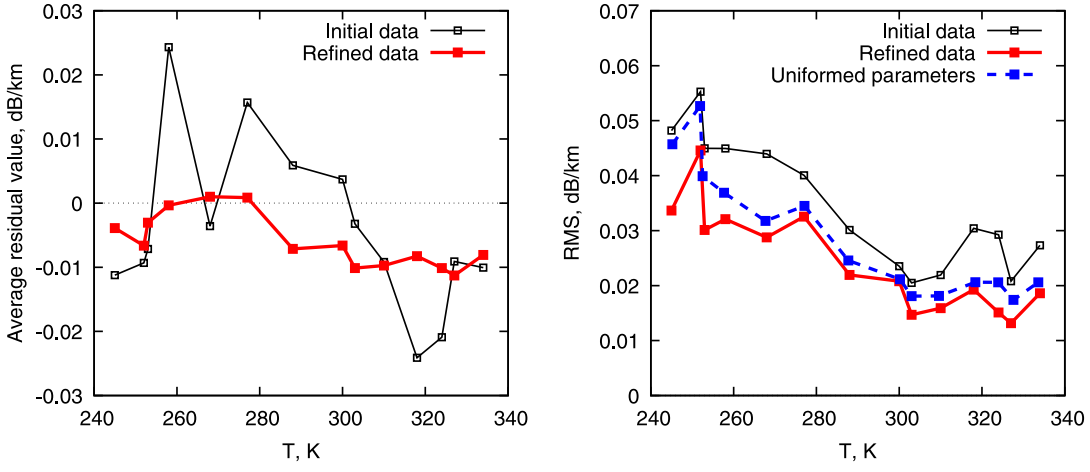

Fig. 11. ECS recording-by-recording fit results for refined and initial ([10,29]) data: mean value of the optimization residual vs. temperature (left) and residuals' standard deviation (right). The uniformed parameters are averaged over temperature.

The difference between calculated and measured band profiles and the "reference" difference from the earlier dataset are shown in Fig. 13. As a reference, the recording at the closest temperature of 300.2 K was chosen. Fig. 13 demonstrates that deviations of the models from experimental recordings obtained using different experimental setups and different sample preparation methods look very similar, even comparing earlier recordings at 750 Torr with the new ones at 1000 Torr. This confirms that both models are capable of accounting for most of the collisional-coupling contribution to the 60-GHz band shape. The obs.-calc. differences have similar magnitudes but a slightly different shape. This shape reproduces at 750 and 1000 Torr for each model, which suggests that this kind of deviation is related to the features of the models, not to measurement imperfections. The major reason for this shape difference between the ECS and MPM calculations is neglecting of the interbranch coupling in the latter (see [10] for details). This

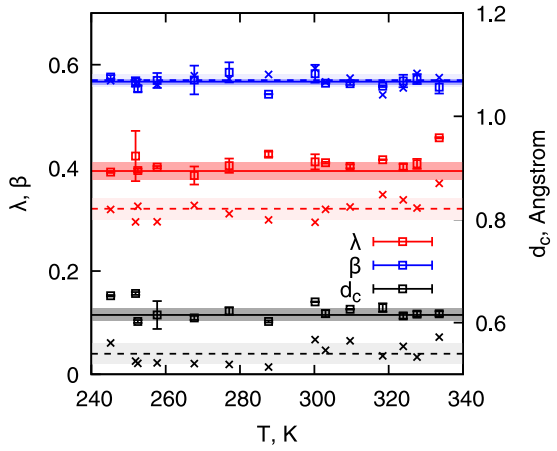

Fig. 12. Parameters of the ECS model derived from recording-by-recording fitting (squares) and their averaged value (solid lines). Standard deviation intervals are shown by error bars of the corresponding color. Values from [10] are shown by crosses (error bars are not shown for those data for the figure clarity) and dotted lines for averaged values.

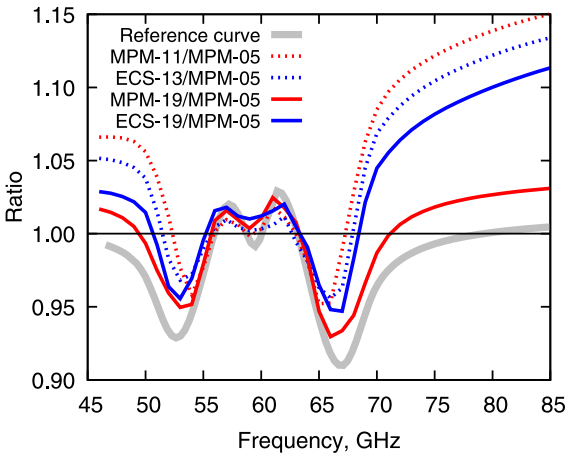

Fig. 14. Ratios of the absorption calculated by MPM-11 [29] and ECS-13 [10] to absorption calculated with MPM-05[18], together with the corresponding ratios for the revised MPM and ECS. The ratio of the revised MPM with mixing corrections up to the second-order to the same model with only first-order corrections is given as a reference.

is the most probable reason for slightly better performance of the ECS model in the range of the band wings around 55 and 65 GHz. Part of the observed systematic difference might be related to the neglected (by both models) speed dependence of collisional relaxation [26]. Its influence was recently revealed for the 118-GHz fine structure O_2 line [4], which is collisionally coupled with the 60-GHz band.

The updated models are in better agreement with the radiometry-validated [34] MPM-05 in the low wing below 51.25 GHz (Fig. 14). The observed deviation of the new models from MPM-05 in the range 52–70 GHz is due to second-order mixing, which was not taken into account in MPM-05 (the expected deviation is shown in Fig. 14 by the grey curve).

Laboratory data in the range 180–260 GHz from [44] at temperature down to 230 K and pressure up to 3 atm provides another comparison. Monomolecular absorption was calculated from these data as a difference between measured total absorption of the dry air and collision-induced absorption (CIA) in dry N_2 multiplied by a factor of 0.84 to take into account different collision efficiency between N_2 and O_2 molecules (see [45] and [46] for details). For the comparison we selected data where the manifestation of the line-mixing effect is more prominent. Corresponding experimental points (see Fig. 17 from [44]) are shown in Fig. 15 together with the smooth approximating function from the same study [44] and our model calculations. Both earlier and revised MPM versions overestimate the absorption but the deviation from the revised model is smaller by nearly a factor of two. The ECS

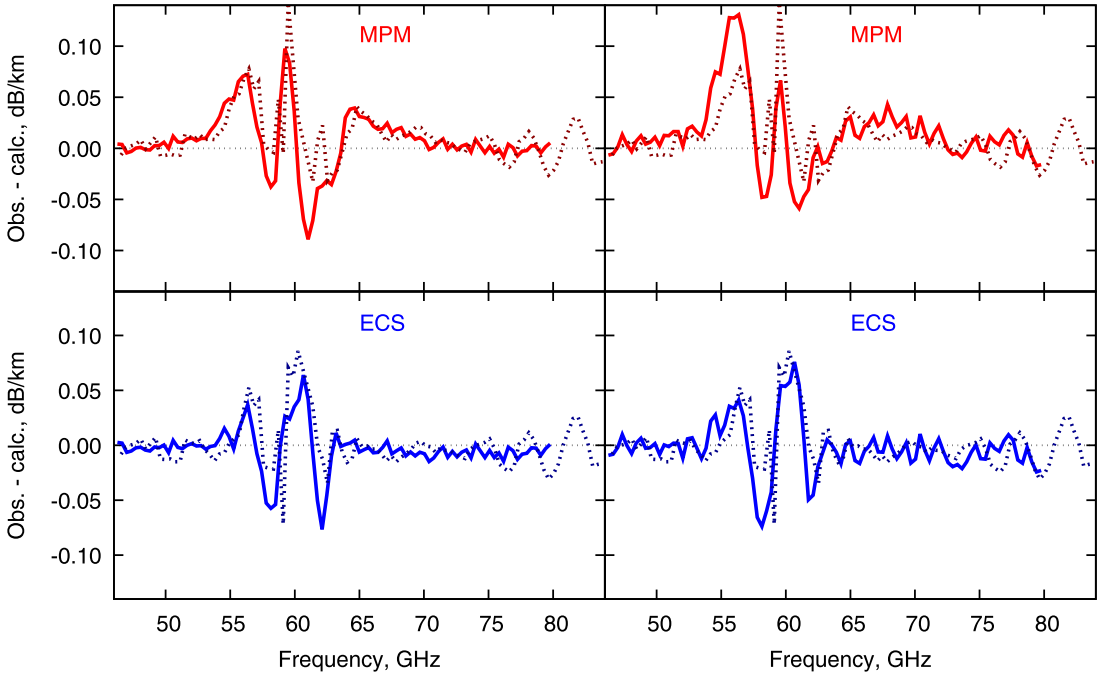

Fig. 13. Difference between measured and calculated profiles of the 60-GHz band. Solid red (for MPM) and blue (for ECS) curves correspond to new recordings at 750 (left) and 1000 Torr (right). Dotted curves show the "reference" difference for the recording at 300.2 K and 748 Torr from the earlier dataset [29], refined in this study. (For interpretation of the references to color in this figure legend, the reader is referred to the web version of this article.)

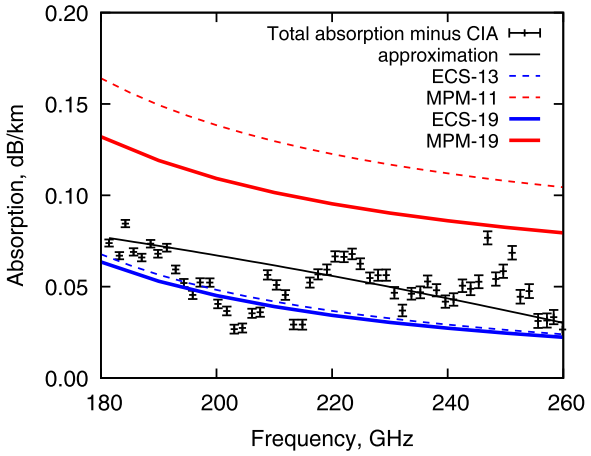

Fig. 15. Monomolecular O_2 absorption in dry air calculated by MPM-11 [29], ECS-13 [10], currently revised MPM and ECS, and the approximation to measurements from [44], for dry air at 3 atm and 230 K.

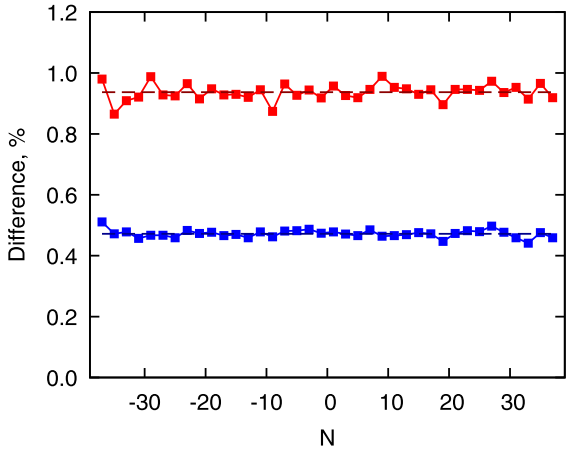

Fig. 16. Relative difference between O_2 fine-structure line intensities: HITRAN-2008 to HITRAN-2004 (blue points) and HITRAN-2016 to HITRAN-2004 (red points) versus line notation. Averaged differences of 0.937 and 0.472 are shown by dashed lines. (For interpretation of the references to color in this figure legend, the reader is referred to the web version of this article.)

model demonstrates even better agreement with the experiment; it behaves more stably and the difference between earlier and revised versions in this frequency range is small.

3. Evaluation of modelling uncertainties

3.1. Band intensity

Known and quite reliable intensity values for the fine structure lines constituting the band were calculated from measured intensities of the lines of the oxygen molecule electronic-vibrational bands [47]. However, corresponding HITRAN values differ from version to version. Comparison of the intensities published in HITRAN-2016 [48], HITRAN-2008 [49] and HITRAN-2004 [50] reveals systematic differences (Fig. 16). Newer intensities are each time about 0.45% larger than the previous version. Small variations of the intensity ratio between neighboring lines are likely due to refinement of the transition frequency or energy of the lower level. The much larger systematic increase of the total band intensity is a more serious change. It might originate from some uniform value which is the same for all lines (such as the partition function). The increasing intensity trend points to the possible presence of systematic imperfections in the calculations. Moreover, the latest version of the HITRAN database [48] does not refer to the published studies related to those intensity calculations or measurements, so the reason for these systematic changes is not clear.

Table 2
Comparison of the 1− line integrated intensity values. Intensities referred to databases are obtained as a sum of the corresponding fine-structure transitions of the main isotopologue in ground and first vibrational state and various isotopologues in the ground state included in the database.

Origin	Value, 10^{-25} cm/molec
Measured [4]	0.9976(37)
HITRAN2004 [50]	0.9933
HITRAN2008 [49]	0.9984
HITRAN2012, 2016 [48,51]	1.00375

Both intensity changes demonstrated in Fig. 16 are much less than the 10–20% uncertainty interval given in HITRAN. But analysis of existing laboratory and radiometric data suggests that such uncertainty is much too large. An uncertainty of 2% was accepted for the band intensity in [34] and it was further reduced to 1% in a recent study [36]. However, the reduced uncertainty is still larger than the intensity corrections in the recent versions of HITRAN.

The insignificant deviations of relative intensities of the individual lines allow calibration of the whole band intensity using the 1− line at 118.75 GHz as a reference point. This line has the same physical origin as the band but it is located apart from the band and other oxygen lines and can be studied separately even at atmospheric pressures. Comparing the directly measured intensity of this line with the corresponding values from databases, we can adjust the intensity of the other fine structure lines to correct the band intensity. In the recent study [4], the 1− line profile was measured at four pressure values by means of the resonator spectrometer [43]. Averaged and recalculated to 296 K, the integrated intensity value of the observed profile was determined as $0.9976(37) \cdot 10^{-25}$ cm/mol. (the uncertainty is given in accordance with Table 2 of [4] providing the complete error budget, including uncertainties of pressure and temperature in the experiment). In the experiment, an oxygen sample of 99.999% declared purity was used, but the isotopic content was natural. This means that the observed line profile is a sum of profiles corresponding to the 1− transition of the main isotopologue $^{16}O_2$ in the ground vibrational state, the similar fine-structure transition in the collisionally-excited vibrational state, and similar transitions of other isotopologues in ground and excited vibrational states. All these transitions have close frequencies (the difference is several orders of magnitude less than the half-width of the line at experimental conditions) so the resulting profile can be treated as a single line profile. Consequently, it is necessary to compare the measured value with the sum of intensities of all related transitions included in the databases.

As follows from Table 2, the nearest to the measured intensity value is given by HITRAN-2008 [49]. Values from HITRAN-2004 and HITRAN-2016 are also very close, but the latter slightly exceeds the experimental uncertainty interval and shows nearly 0.5% relative difference (which is half the uncertainty evaluation from [36]). Analysis of these data suggests that the uncertainty of the band intensity of ∼1% is still overestimated and can be further reduced to the interval of the measured $N = 1-$ line intensity, corresponding to the uncertainty of ∼0.37%. This value will be applied below to evaluate the uncertainty of MPM and ECS model calculations.

3.2. Models' parameters correlation and calculation uncertainty

It was shown in [36] that proper evaluation of the model uncertainty should include analysis of the model parameters' covari-

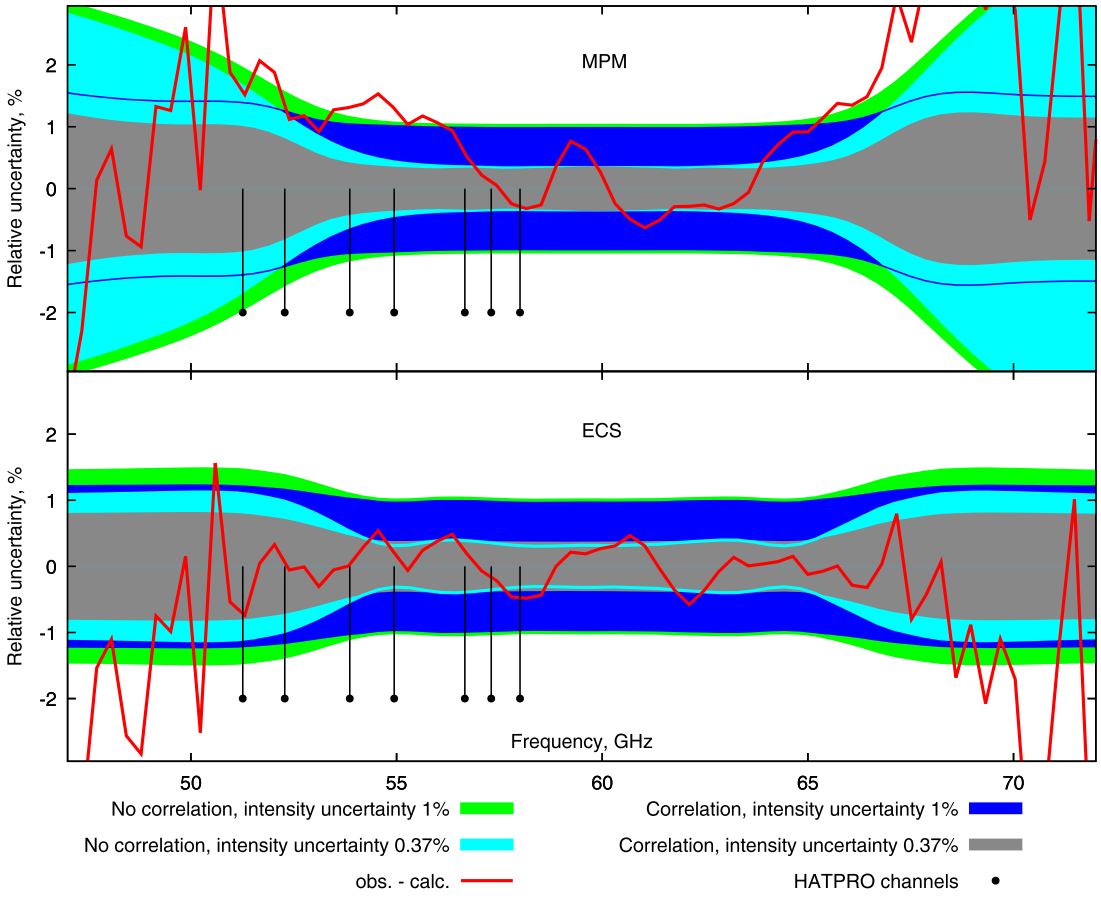

Fig. 17. Uncertainties of the 60-GHz band profile calculated with the MPM and ECS at 300 K and 750 Torr, together with the relative obs.-calc. residual of the recording taken at the same conditions.

ance. A detailed description of method and expressions used for the evaluation can be found in the supplementary materials. In this section we present only a short description of the evaluation approach and results.

Covariances of the whole set of MPM parameters (Table 1) were found using a Monte-Carlo method through analysis of the pseudo-experimental recordings generated as calculated band profiles, with addition of normally distributed noise of the same magnitude as random instrumental noise in the experiment (0.01 dB/km). For each calculated profile, randomized values with the corresponding expected values and standard deviations were used for all parameters with known uncertainties. Covariances of temperature independent Z^0 and Z^1 mixing parameters were found analytically using well-known equations.

Covariances of the ECS model parameters were also found analytically using an approach similar to sections 30 and 31 of Chapter 7 in [52].

The relative uncertainties of the absorption calculated by MPM and ECS are shown in Fig. 17. For both models, accounting for the parameters' uncertainty covariances is almost negligible near the band center, but at the wings it decreases total calculation uncertainty. It is seen that 1% uncertainty of the integrated intensity of the band dominates over uncertainties of all other parameters. In this case the difference between observed and calculated absorption lies within the area of the calculation uncertainty, though it still looks systematic in the vicinity of the band center. As a result, the shape of the band is known with more accuracy than the intensity. The contribution of the band-intensity uncertainty is comparable with that of the shape-controlling parameters when its value decreases down to 0.37% in accordance with subsection 3.1. The corresponding decrease of the uncertainty is quite noticeable, including the range on the lower wing of the band from 50 to 55 GHz, which is of special interest for radiometry [34,36] (positions of the HATPRO radiometer channels widely used in atmospheric remote sensing are also shown in Fig. 17). The origin of the greater MPM calculation uncertainty in the band wings is due to the increasing uncertainties of mixing parameters derived from the experimental data with increasing N (Table 1 and Fig. 9), which results in greater absorption uncertainty, especially when correlation is ignored.

4. Discussion and conclusions

Models using two different approaches to describe the molecular oxygen 60-GHz band shape were revised and updated on the basis of refined experimental data. We demonstrated that MPM and ECS with updated empirical parameters provide comparable accuracy of reproduction of the experimental data they are based on, with a minor advantage for the ECS approach. This seems quite reasonable, as both models have comparable degrees of freedom, but the ECS approach has fewer simplifying assumptions. The difference between these two approaches to the band-profile calculation is seen mostly in the shape of the systematic residual between observed and calculated absorption. This conclusion is confirmed by the fact that recordings obtained about ten years later with the newer version of the resonator spectrometer provide similar-looking systematic residuals. Both improved models were validated in the range of the 60-GHz band wings by earlier radiometric (near 51 GHz) and laboratory (180–260 GHz) data.

Table 3
Standard deviation of the obs.-calc. absorption difference for various versions of MPM.

MPM version (by year)	Obs.-calc. st.dev. at 300 K, dB/km
1989 [53]	0.27
1992 [16]	0.18
2005 [18]	0.1
2011 [29]	0.05
current version	0.025

The modeling progress for MPM is shown in Table 3: each successive version, including the current update, shows 1.5 to 2 times smaller obs.-calc. standard deviation compared to the previous one.

Additionally, it was shown that total uncertainty of the calculated absorption depends not only on the individual uncertainties of the models' parameters derived from experimental data, but also on the covariances between these parameters. For both models the contribution of the collisional parameters' uncertainties is noticeable. At the same time the impact of the uncertainty of the band intensity dominates over all other sources of uncertainty unless the intensity uncertainty is reduced to 0.37%, which does seem justified, taking into account accurate experimental data on the 118-GHz line [4] and results of theoretical calculations (Fig. 17).

Declaration of Competing Interest

The authors declare that they have no known competing financial interests or personal relationships that could have appeared to influence the work reported in this paper.

CRediT authorship contribution statement

Dmitriy S. Makarov: Data curation, Formal analysis, Writing - original draft. **Mikhail Yu. Tretyakov:** Conceptualization, Validation, Writing - review & editing. **Philip W. Rosenkranz:** Conceptualization, Methodology, Writing - review & editing.

Acknowledgement

Studies on the data-treatment method, experimental-recordings refinement, and related to the band intensity are supported by State Project 0035-2019-0016. Test-measurements methods development, models revision and their uncertainty evaluation are supported by Russian Science Foundation grant 18-72-10113.

The authors are grateful to the reviewers for valuable comments which helped to improve the manuscript.

Supplementary material

Supplementary material associated with this article can be found, in the online version, at 10.1016/j.jqsrt.2019.106798

References

[1] Anderson RS, Johnson CM, Gordy W. Resonant absorption of oxygen at 2.5-millimeter wavelength. Phys Rev 1951;83:1061–2.
[2] Schulze AE, Tolbert CW. Shape, intensity and pressure broadening of the 2.53-millimetre wave-length oxygen absorption line. Nature 1963;200(4908):747–50.
[3] Rosenkranz PW. Shape of the 5 mm oxygen band in the atmosphere. IEEE Trans Antennas Propag 1975;23(4):498–506.
[4] Koshelev MA, Delahaye T, Serov EA, Vilkov IN, Boulet C, Tretyakov MY. Accurate modeling of the diagnostic 118-ghz oxygen line for remote sensing of the atmosphere. J Quant Spectrosc Rad Transfer 2017;196(Supplement C):78–86. doi:10.1016/j.jqsrt.2017.03.043.
[5] Baranger M. Problem of overlapping lines in the theory of pressure broadening. Phys Rev 1958;111(2):494–504.
[6] Kolb AC, Griem H. Theory of line broadening in multiplet spectra. Phys Rev 1958:514–21.
[7] Fano U. Pressure broadening as a prototype of relaxation. Phys Rev 1963;131(1):259–68.
[8] Gordon RG. On the pressure broadening of molecular multiplet spectra. J Chem Phys 1967;46(2):448–55.
[9] Smith EW. Absorption and dispersion in the O_2 microwave spectrum at atmospheric pressures. J Chem Phys 1981;74(12):6658–73.
[10] Makarov DS, Tretyakov MY, Boulet C. Line mixing in the 60-GHz atmospheric oxygen band: comparison of the MPM and ECS model. J Quant Spectrosc Rad Transfer 2013;124:1–10.
[11] Hill R, Gordy W. Zeeman effect and line breadth studies of the microwave lines of oxygen. Phys Rev 1954;93(5):1019–22.
[12] Gimmestad GG, Llewellyn-Jones DT, Gebbie HA. Millimetre wave oxygen attenuation measurements. J Quant Spectrosc Radiat Transfer 1976;16:899–900.
[13] Setzer BJ, Pickett HM. Pressure broadening measurements of the 118.750 GHz oxygen transition. J Chem Phys 1977;67:340–3.
[14] Pickett HM, Cohen EA, Brinza DE. Pressure broadening and its implications for cosmic background measurements. Astrophys J 1981;248:L49–51.
[15] Read WG, Hillig KW, Cohen EA, Pickett HM. The measurement of absolute absorption of millimeter radiation in gases : the absorption of CO and O_2. IEEE Trans Anten Propag 1988;36(8):1136–43.
[16] Liebe HJ, Rosenkranz PW, Hufford GA. Atmospheric 60-GHz oxygen spectrum: new laboratory measurement and line parameters. J Quant Spectrosc Rad Transfer 1992;48(5,6):629–43.
[17] Tretyakov MY, Golubiatnikov GY, Parshin VV, Koshelev MA, Myasnikova SE, Krupnov AF, et al. Experimental study of the line mixing coefficient for 118.75 GHz oxygen line. J Molec Spectrosc 2004;223:31–8.
[18] Tretyakov MY, Koshelev MA, Dorovskikh VV, Makarov DS, Rosenkranz PW. 60-GHz oxygen band: precise broadening and central frequencies of fine structure lines, absolute absorption profile at atmospheric pressure, revision of mixing coefficients. J Molec Spectrosc 2005;231:1–14.
[19] Tretyakov MY, Koshelev MA, Koval I, Parshin VV, Kukin LM, Fedoseev LI, et al. Temperature dependence of pressure broadening of the $N = 1-$ fine structure oxygen line at 118.75 GHz. J Molec Spectrosc 2007;241(1):109–11.
[20] Drouin BJ. Temperature dependent pressure induced linewidths of $^{16}O_2$ and $^{18}O^{16}O$ transitions in nitrogen, oxygen and air. J Quant Spectrosc Rad Transfer 2007;105(3):450–8.
[21] Makarov DS, Koval IA, Koshelev MA, Parshin VV, Tretyakov MY. Collisional parameters of the 118-GHz oxygen line: temperature dependence. J Molec Spectrosc 2008;252:242–3.
[22] Koshelev MA, Vilkov IN, Tretyakov MY. Collisional broadening of oxygen fine structure lines: the impact of temperature. J Quant Spectrosc Rad Transfer 2016;169:91–5.
[23] Lam KS. Application of pressure broadening theory to the calculation of atmospheric oxygen and water vapor microwave absorption. J Quant Spectrosc Rad Transfer 1977;17:351–83.
[24] DePristo A, Augustin S, Ramaswamy R, Rabitz H. Quantum number and energy scaling for nonreactive collisions. J Chem Phys 1979;71:850–65.
[25] Tran H, Boulet C, Hartmann J-M. Line mixing and collision-induced absorption by oxygen in the A-band: laboratory measurements, model, and tools for atmospheric spectra computations. J Geophys Res 2006;111:D15210.
[26] Hartmann J-M, Boulet C, Robert D. Collisional effects on molecular spectra. Elsevier; 2008.
[27] Liebe HJ, Gimmestad GG, Hopponen JD. Atmospheric oxygen microwave spectrum—experiment versus theory. IEEE Trans Antennas Propag 1977;25(3):327–35.
[28] Rosenkranz PW. Interference coefficients for overlapping oxygen lines in air. J Quant Spectrosc Rad Transfer 1988;39:281–97.
[29] Makarov DS, Tretyakov MY, Rosenkranz PW. 60-Ghz oxygen band: precise experimental profiles and extended absorption modeling in a wide temperature range. J Quant Spectrosc Rad Transfer 2011;112(9):1420–8.
[30] Rosenkranz P.W., Line-by-line microwave radiative transfer (non-scattering). URL https://www.doi.org/10.21982/M81013.
[31] Twomey S. On the numerical solution of Fredholm integral equations of the first kind by the inversion of the linear system produced by quadrature. J ACM 1963;10(1):97–101.
[32] Tikhonov AN. On the solution of incorrectly stated problems and a method of regularization. Dokl Akad Nauk SSSR 1963;151:501–4.
[33] Tikhonov AN. On the regularization of ill-posed problems. Dokl Akad Nauk SSSR 1963;153:49–52.
[34] Cadeddu MP, Payne VH, Clough SA, Cady-Pereira K, Liljegren JC. Effect of the oxygen line-parameter modeling on temperature and humidity retrievals from ground-based microwave radiometers. IEEE TransGeosciRemote Sens 2007;45(7):2216–23.
[35] Tretyakov MY, Krupnov AF, Koshelev MA, Makarov DS, Serov EA, Parshin VV. Resonator spectrometer for precise broadband investigations of atmospheric absorption in discrete lines and water vapor related continuum in millimeter wave range. Rev Sci Instrum 2009;80:093106-1–10.
[36] Cimini D, Rosenkranz PW, Tretyakov MY, Koshelev MA, Romano F. Uncertainty of atmospheric microwave absorption model: impact on ground-based radiometer simulations and retrievals. Atmos Chem Phys 2018;18(20):15231–59.
[37] Makarov D.S, Tretyakov M.Yu., Rosenkranz P.W.Data for: rRevision of the 60-Ghz atmospheric oxygen absorption band models for practical use (version 2).2019. URL https://data.mendeley.com/datasets/xbz9f3px9p/2. doi:10.17632/xbz9f3px9p.2.

[38] Van Vleck JH, Weisskopf VF. On the shape of collision-broadened lines. Rev Mod Phys 1945;17:227–36.
[39] Niro F, Boulet C, Hartmann J-M. Spectra calculations in central and wing regions of CO_2 IR bands between 10 and 20 μm. I: Model and laboratory measurements. J Quant Spectrosc Rad Transfer 2004;88:483–98.
[40] Millot G. Rotationally inelastic rates over a wide temperature range based on an energy corrected sudden-exponential–power theoretical analysis of Raman line broadening coefficients and Q branch collapse. J Chem Phys 1990;93(11):8001–10. doi:10.1063/1.459329.
[41] Brunner TA, Pritchard D. Dynamics of the excited state. In: Advances in chemical Physics, L. John Wiley & Sons Ltd; 1982. p. 589–641. ISBN 9780470142745.
[42] Levenberg K. A method for the solution of certain non-linear problems in least squares. Quart Appl Math 1944;2:164–8.
[43] Koshelev MA, Leonov II, Serov EA, Chernova AI, Balashov AA, Bubnov GM, et al. New frontiers in modern resonator spectroscopy. IEEE Trans Terahertz SciTechnol 2018;8(6):773–83. doi:10.1109/TTHZ.2018.2875450.
[44] Meshkov AI, De Lucia FC. Laboratory measurements of dry air atmospheric absorption with a millimeter wave cavity ringdown spectrometer. J Quant Spectrosc Rad Transfer 2007;108(2):256–76.
[45] Boissoles J, Boulet C, Tipping RH, Brown A, Ma Q. Theoretical calculation of the translation-rotation collision-induced absorption in N_2-N_2, O_2-O_2, and N_2-O_2 pairs. J Quant Spectrosc Rad Transfer 2003;82(1):505–16.
[46] Tretyakov MY, Zibarova AO. On the problem of high-accuracy modeling of the dry air absorption spectrum in the millimeter wavelength range. J Quant Spectrosc Rad Transfer 2018;216:70–5. doi:10.1016/j.jqsrt.2018.05.008.
[47] Gamache RR, Goldman A, Rothman LS. Improved spectral parameters for the three most abundant isotopomers of the oxygen molecule. J Quant Spectrosc Rad Transfer 1998;59(3):495–509.
[48] Gordon IE, Rothman LS, Hill C, Kochanov RV, Tan Y, Bernath PF, et al. The HITRAN2016 molecular spectroscopic database. J Quant Spectrosc Rad Transfer 2017;203:3–69.
[49] Rothman LS, Gordon IE, Barbe A, Benner DC, Bernath PF, Birk M, et al. The HITRAN2008 molecular spectroscopic database. J Quant Spectrosc Rad Transfer 2009;110(9):533–72.
[50] Rothman LS, Jacquemart D, Barbe A, Benner DC, Birk M, Brown LR, et al. The HITRAN2004 molecular spectroscopic database. J Quant Spectrosc Rad Transfer 2005;96(2):139–204.
[51] Rothman LS, Gordon IE, Babikov Y, Barbe A, Benner DC, Bernath PF, et al. The HITRAN2012 molecular spectroscopic database. J Quant Spectrosc Rad Transfer 2013;130:4–50.
[52] van der Waerden BL. Mathematical statistics. 1st ed. Springer-Verlag Berlin Heidelberg; 1969.
[53] Liebe HJ. MPM — an atmospheric millimeter-wave propagation model. Int J Infrared Mill Waves 1989;10:631–50.